 CMES, vol.4, no.6, pp.665-678, 2003

Truly Meshless Local Petrov-Galerkin (MLPG) Solutions of Traction & Displacement BIEs

Z. D. Han[1] **and S. N. Atluri**[1]

Abstract: The numerical implementation of the truly Meshless Local Petrov-Galerkin (MLPG) type weak-forms of the displacement and traction boundary integral equations is presented, for solids undergoing small deformations. In the accompanying part I of this paper, the general MLPG/BIE weak-forms were presented [Atluri, Han and Shen (2003)]. The MLPG weak forms provide the most general basis for the numerical solution of the non-hyper-singular displacement and traction BIEs [given in Han, and Atluri (2003)], which are simply derived by using the gradients of the displacements of the fundamental solutions [Okada, Rajiyah, and Atluri (1989a,b)]. By employing the various types of test functions, in the MLPG-type weak-forms of the non-hyper-singular dBIE and tBIE over the local sub-boundary surfaces, several types of MLPG/BIEs are formulated, while also using several types of non-element meshless interpolations for trial functions over the surface of the solid. Specifically, three types of MLPG/BIEs are formulated in that paper, i.e. MLPG/BIE1, MLPG/BIE2, and MLPG/BIE6, as per the consistent categorizations of the MLPG domain methods [Atluri and Shen (2002a)]. As the accompanying part II, this paper is devoted to MLPG/BIE6. In particular, the moving least squares (MLS) method has been extended for the approximation on three dimensional surfaces, which makes it possible for the MLPG/BIE methods to be truly meshless. Numerical examples, including crack problems, are presented to demonstrate that the present methods are very promising, especially for solving the elastic problems in which the singularities in displacements, strains, and stresses, are of primary concern.

keyword: Meshless Local Petrov-Galerkin approach (MLPG), Boundary Integral Equations (BIE), Non-Hypersingular dBIE/tBIE, Moving Least Squares (MLS), MLPG/BIE.

[1] Center for Aerospace Research & Education
University of California, Irvine
5251 California Avenue, Suite 140
Irvine, CA, 92612, USA

1 Introduction

The meshless local Petrov-Galerkin (MLPG) approach has become very attractive as a very promising method for solving partial differential equations. The MLPG method was originally applied for domain discretizations in Atluri and Zhu (1998). The main advantage of this method over the widely used finite element methods is that it does not need any mesh either for the interpolation of the solution variables or for the integration of the weak forms. The MLPG approach is very general, and can be based on the symmetric or unsymmetric local weak-forms of the PDEs, and uses a variety of interpolation methods (trial functions), test functions, integration schemes with/without background cells, and their flexible combinations. Such generality has been widely investigated [Atluri and Shen (2002a,b)]. The many research successes in solving PDEs, demonstrate that the MLPG method, and its variants, become some of the most promising alternative methods for computational mechanics.

The boundary integral equations (BIEs) have also been developed for solving PDEs, because of their efficiency in certain applications, in comparison to the domain-solution methods. They have been applied to solve linear elastic isotropic solid mechanics problems [Okada, Rajiyah, and Atluri (1990)], 3-D dynamic problems [Hatzigeorgiou, and Beskos (2002)], cracked plate problems [Wen, Aliabadi, and Young (2003), El-Zafrany (2001)], acoustic problems [Gaul, Fischer,and Nackenhorst (2003)], and biological systems [Muller-Karger, Gonzalez, Aliabadi and Cerrolaza] (2001)]. It is well known that the hyper-singularities of the traction BIEs, as derived directly from differentiating the displacement BIEs, hinder their applications in various numerical implementations. The hyper-singular BIEs need some spe-

cial treatments, such as the various de-singularization techniques [Richardson and Cruse (1996)]. In contrast, as far back as 1989, Okada, Rajiyah, and Atluri (1989a,b, 1990) have proposed a simple way to *directly derive* the integral equations for the gradients of displacements. It resulted in "non-hyper-singular" boundary integral equations for the gradients of displacements, and these have been applied to solve the nonlinear problems successfully. Recently, this concept has been followed and extended for a *directly-derived* traction BIE [Han and Atluri (2002, 2003)], which is also "non-hyper-singular" [$1/r^2$], as opposed to being "hyper-singular" [$1/r^3$]. Han and Atluri (2003) have also proposed a very straightforward and simple procedure to de-singularize the "non-hyper-singular" integrals, in order to render them numerically tractable, with only a weak singularity. These weakly-singular dBIE and tBIE are solved here by using the MLPG approaches, by writing their local weak-forms in the local sub-boundary surfaces. These meshless solution methods for solving BIEs are labeled as MLPG/BIE approaches. The generalities of the MLPG/BIE approaches have been discussed in the accompanying part I of the paper [Atluri, Han and Shen (2003)], in which various forms of MLPG/BIEs were proposed. Some issues in the numerical implementation have also been addressed there.

In the present paper, we implement the formulations proposed in Atluri, Han and Shen (2003) for the MLPG/BIE6 and solve some elastic problems, including fracture mechanics problems of non-planar crack-growth. The MLS method is used to construct the interpolation functions on the surface of a three-dimensional body. It is well unknown that the moment matrix becomes singular or nearly singular, if the 3-D Cartesian coordinates are used in the MLS over a general 3-D surface. For three dimensional surface cases, the curvilinear coordinates are used in the boundary node method (BNM) [Gowrishankar and Mukherjee (2002)], in which the background cells are required for the approximation, as well as for the integration. It prevents the meshless BIE methods to be truly meshless, since it still involves the mesh generation and re-meshing. As an alternate implementation, the varying polynomial basis may be chosen, with the use of Cartesian coordinates, so that the singularity in the MLS is eliminated, as proposed for the boundary cloud method (BCM) [Li and Aluru (2003)]. However, it is difficult to choose the polynomial basis for the arbitrary 3D surfaces. Secondly, the local geometry information is required to help in choosing the basis. The idea of the varying basis is promising, but is difficult for the numerical implementation, as worse results were reported by the authors [Li and Aluru (2003)]. In the present paper, we check the singularity of the moment matrix, and determine the local normal direction of 3D surfaces from its lowest eigenvector. Then, the singularity of the moment matrix has been cancelled, by using this information on the local normal direction. *With this extension, the local geometry information or the background cells are not required for the MLS, to construct the interpolation functions.* It leads to truly meshless BIE methods, if the integration schemes are based on nodal influence domains, as discussed in [Atluri, Han and Shen (2003)]. In this paper, we focus on the displacement and traction MLPG/BIEs in their local symmetric weak-forms, with the combination of the enhanced MLS surface interpolation method.

The outline of the paper is as follows: Section 2 summarizes the non-hypersingular displacement and traction BIEs [Han and Atluri (2003)], and their MLGP approaches [Atluri, Han and Shen (2003)]; In Section 3, the MLS approximation is extended to recondition the singular or nearly singular moment matrix when it is applied for the approximation over the three dimensional surface; Section 4 discusses the numerical results by using the moving least squares in the MLPG/BIE6 method. Some conclusions are made in Section 5.

2 Non-Hyper-singular MLPG Displacement and Traction BIEs

This section summarizes, for the sake of completeness, the non-hypersingular MLPG displacement and traction BIEs for a linear elastic, homogeneous, isotropic solid. They were proposed and discussed in detail in [Atluri, Han and Shen (2003)], by extending the general non-hyper-singular dBIE and tBIEs through the MLPG approaches [Han and Atluri (2003)].

2.1 BIEs for elastic problems

Consider a linear elastic, homogeneous, isotropic body in a domain Ω, with a boundary $\partial\Omega$. The Lame' constants of the linear elastic isotropic body are λ and μ; and the corresponding Young's modulus and Poisson's ratio are E and υ, respectively. We use Cartesian coordinates ξ_i,

and the attendant base vectors $\mathbf{e}_i$, to describe the geometry in Ω. The solid is assumed to undergo infinitesimal deformations. The equations of balance of linear and angular momentum can be written as:

$$\boldsymbol{\nabla}\cdot\boldsymbol{\sigma}+\mathbf{f}=\mathbf{0};\quad \boldsymbol{\sigma}=\boldsymbol{\sigma}^{\mathrm{t}};\quad \boldsymbol{\nabla}=\mathbf{e}_i\frac{\partial}{\partial\xi_i} \tag{1}$$

The strain-displacement relations are:

$$\boldsymbol{\varepsilon}=\frac{1}{2}(\boldsymbol{\nabla}\mathbf{u}+\mathbf{u}\boldsymbol{\nabla}) \tag{2}$$

The constitutive relations of an isotropic linear elastic homogeneous solid are:

$$\boldsymbol{\sigma}=\lambda\mathbf{I}(\boldsymbol{\nabla}\cdot\mathbf{u})+2\mu\boldsymbol{\varepsilon} \tag{3}$$

The forms of the boundary integral equations, which are used in the present paper, are given by [Han and Atluri 2003], for displacement,

$$\begin{aligned} u_p(\mathbf{x}) &= \int_{\partial\Omega} t_j(\xi)u_j^{*p}(\mathbf{x},\xi)\,dS \\ &\quad -\int_{\partial\Omega} n_i(\xi)u_j(\xi)\sigma_{ij}^{*p}(\mathbf{x},\xi)\,dS \end{aligned} \tag{4a}$$

and for traction

$$\begin{aligned} -t_b(\mathbf{x}) &= \int_{\partial\Omega} t_q(\xi)n_a(\mathbf{x})\sigma_{ab}^{*q}(\mathbf{x},\xi)\,dS \\ &\quad +\int_{\partial\Omega} D_p u_q(\xi)n_a(\mathbf{x})\Sigma_{abpq}^{*}(\mathbf{x},\xi)\,dS \end{aligned} \tag{4b}$$

where u_j^{*p}, σ_{ij}^{*p} and Σ_{abpq}^{*} are kernel functions, which were first given in Han and Atluri (2003) and listed in the appendix for 2D and 3D problems separately; the surface tangential operator D_t is defined as,

$$D_t = n_r e_{rst}\frac{\partial}{\partial\xi_s} \tag{5}$$

It should be pointed out that dBIE and tBIE in Eq. (4) are directly derived without hyper-singularities, as originally presented in [Okada, Rajiyah, and Atluri (1989a,b)]. They are both numerically tractable after desingulariztion by using the identities of the fundamental solution [Han and Atluri (2003)].

2.2 MLPG Approaches

The meshless approach for solving PDEs has attracted much attention during the past decades. As a general method, the MLPG approach was first proposed by Atluri and Zhu (1998) for solving linear potential problems, by using either a local symmetric weak form, or an unsymmetric weak form of the governing equation *over the local sub domain, and such local domains may overlap each other*. The generality of the MLPG, and its variants, are comprehensively investigated in Atluri and Shen (2002a,b). This approach can also be used for solving BIEs, instead of using traditional element-based methods, such as the Boundary Element Method. Following the general idea as presented in Atluri and Zhu (1998), one may consider a local sub-boundary surface $\partial\Omega_L$, with its boundary contour Γ_L, as a part of the whole boundary-surface, as shown in Figure 1, for a 3-D solid. Eq. (4) may be satisfied in weak-forms over the sub-boundary surface $\partial\Omega_L$, by using a Local Petrov-Galerkin scheme, as:

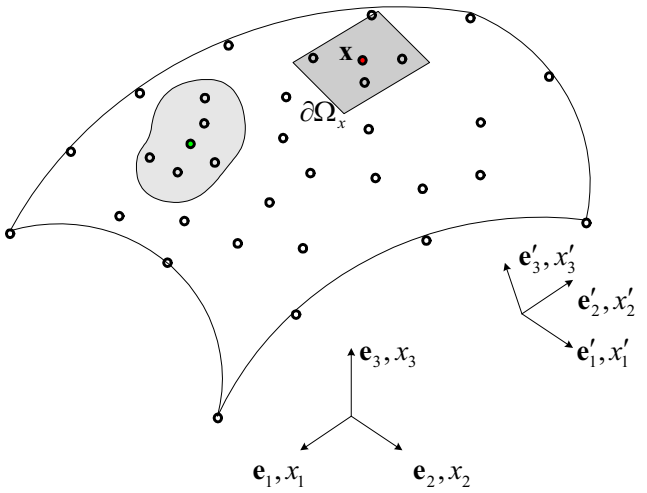

Figure 1 : A sub-part of the boundary around point **x**

$$\begin{aligned} &\int_{\partial\Omega_L} w_p(\mathbf{x})u_p(\mathbf{x})dS_x \\ &\quad = \int_{\partial\Omega_L} w_p(\mathbf{x})dS_x \int_{\partial\Omega} t_j(\xi)u_j^{*p}(\mathbf{x},\xi)\,dS \\ &\quad -\int_{\partial\Omega_L} w_p(\mathbf{x})dS_x \int_{\partial\Omega} n_i(\xi)u_j(\xi)\sigma_{ij}^{*p}(\mathbf{x},\xi)\,dS \end{aligned} \tag{6a}$$

$$
\begin{aligned}
&-\int_{\partial\Omega_L} w_b(\mathbf{x}) t_b(\mathbf{x}) dS_x \\
&\quad = \int_{\partial\Omega_L} w_b(\mathbf{x}) dS_x \int_{\partial\Omega} t_q(\xi) n_a(\mathbf{x}) \sigma^{*q}_{ab}(\mathbf{x},\xi)\, dS_\xi \\
&\quad + \int_{\partial\Omega_L} w_b(\mathbf{x}) dS_x \int_{\partial\Omega} D_p u_q(\xi) n_a(\mathbf{x}) \Sigma^{*}_{abpq}(\mathbf{x},\xi)\, dS_\xi
\end{aligned} \tag{6b}
$$

where $\mathbf{w}(\mathbf{x})$ is a vector test function. If $\mathbf{w}(\mathbf{x})$ is chosen as a Dirac delta function, i.e. $w_b(\mathbf{x}) = \delta(\mathbf{x},\mathbf{x}_m)$ at $\partial\Omega_L$, we obtain the standard "collocation" method for displacement and traction BIEs, at the collocation point $\mathbf{x}_m$. Their detail de-singularized forms have been presented in Atluri, Han and Shen (2003). One may also choose $\mathbf{w}(\mathbf{x})$ in such way that it is continuous over the local sub boundary-surface $\partial\Omega_L$ and zero at the contour Γ_L, and apply Stokes' theorem to Eq. (6), and re-write it as:

$$
\begin{aligned}
&\frac{1}{2}\int_{\partial\Omega_L} w_p(\mathbf{x}) u_p(\mathbf{x}) dS_x \\
&\quad = \int_{\partial\Omega_L} w_p(\mathbf{x}) dS_x \int_{\partial\Omega} t_j(\xi) u^{*p}_j(\mathbf{x},\xi)\, dS_\xi \\
&\quad + \int_{\partial\Omega_L} w_p(\mathbf{x}) dS_x \int_{\partial\Omega} D_i(\xi) u_j(\xi) G^{*p}_{ij}(\mathbf{x},\xi)\, dS_\xi \\
&\quad + \int_{\partial\Omega_L} w_p(\mathbf{x}) dS_x \int^{CPV}_{\partial\Omega} n_i(\xi) u_j(\xi) \phi^{*p}_{ij}(\mathbf{x},\xi)\, dS_\xi
\end{aligned} \tag{7a}
$$

$$
\begin{aligned}
&-\frac{1}{2}\int_{\partial\Omega_L} t_b(\mathbf{x}) w_b(\mathbf{x}) dS_x \\
&\quad = \int_{\partial\Omega_L} D_a w_b(\mathbf{x}) dS_x \int_{\partial\Omega} t_q(\xi) G^{*q}_{ab}(\mathbf{x},\xi)\, dS_\xi \\
&\quad - \int_{\partial\Omega} t_q(\xi)\, dS_\xi \int^{CPV}_{\partial\Omega_L} n_a(\mathbf{x}) w_b(\mathbf{x}) \phi^{*q}_{ab}(\mathbf{x},\xi) dS_x \\
&\quad + \int_{\partial\Omega_L} D_a w_b(\mathbf{x}) dS_x \int_{\partial\Omega} D_p u_q(\xi) H^{*}_{abpq}(\mathbf{x},\xi)\, dS_\xi
\end{aligned} \tag{7b}
$$

where G^{*q}_{ab}, ϕ^{*q}_{ab} and H^{*}_{abpq} are fundamental solution related kernel functions and given in the appendix for both 2D and 3D problems.

In the present implementation, the test function $w_b(\mathbf{x})$ is chosen to be identical to a function that is energy-conjugate to u_p (for dBIE) and t_b (for tBIE), namely, the nodal trial function $\hat{t}_p(\mathbf{x})$ and $\hat{u}_b(\mathbf{x})$, respectively, we obtain the local symmetric Galerkin weak-forms of the weakly singular dBIE and tBIE, as:

$$
\begin{aligned}
&\frac{1}{2}\int_{\partial\Omega_L} \hat{t}_p(\mathbf{x}) u_p(\mathbf{x}) dS_x \\
&\quad = \int_{\partial\Omega_L} \hat{t}_p(\mathbf{x}) dS_x \int_{\partial\Omega} t_j(\xi) u^{*p}_j(\mathbf{x},\xi)\, dS_\xi \\
&\quad + \int_{\partial\Omega_L} \hat{t}_p(\mathbf{x}) dS_x \int_{\partial\Omega} D_i(\xi) u_j(\xi) G^{*p}_{ij}(\mathbf{x},\xi)\, dS_\xi \\
&\quad + \int_{\partial\Omega_L} \hat{t}_p(\mathbf{x}) dS_x \int^{CPV}_{\partial\Omega} n_i(\xi) u_j(\xi) \phi^{*p}_{ij}(\mathbf{x},\xi)\, dS_\xi
\end{aligned} \tag{8a}
$$

$$
\begin{aligned}
&-\frac{1}{2}\int_{\partial\Omega_L} t_b(\mathbf{x}) \hat{u}_b(\mathbf{x}) dS_x \\
&\quad = \int_{\partial\Omega_L} D_a \hat{u}_b(\mathbf{x}) dS_x \int_{\partial\Omega} t_q(\xi) G^{*q}_{ab}(\mathbf{x},\xi)\, dS_\xi \\
&\quad - \int_{\partial\Omega} t_q(\xi)\, dS_\xi \int^{CPV}_{\partial\Omega_L} n_a(\mathbf{x}) \hat{u}_b(\mathbf{x}) \phi^{*q}_{ab}(\mathbf{x},\xi) dS_x \\
&\quad + \int_{\partial\Omega_L} D_a \hat{u}_b(\mathbf{x}) dS_x \int_{\partial\Omega} D_p u_q(\xi) H^{*}_{abpq}(\mathbf{x},\xi)\, dS_\xi
\end{aligned} \tag{8b}
$$

3 Meshless Interpolation

The MLS method of interpolation is generally considered to be one of the best schemes to interpolate random data with a reasonable accuracy [Atluri and Zhu (1998)]. Although the nodal shape functions that arise from the MLS approximation have a very complex nature, they always preserve completeness up to the order of the chosen basis, and robustly interpolate the irregularly distributed nodal information. The MLS scheme has been widely used in domain discretization methods [Atluri and Shen (2002b)]. If we consider the MLS approximation on the boundary of a 3D solid domain, i.e., a 3D surface, the moment matrix in the MLS interpolation sometimes becomes singular, if global Cartesian coordinates are used in describing the surface, and if the surface containing the nodes in the domain of influence of the node in question becomes nearly planar. The two surface-curvilinear coordinates may be used here as an alternative choice, but it requires the background cells, which hinders it from being a true meshless implementation. In the present study,

we present a method to recondition the singular moment matrix, while still using the global Cartesian coordinates to approximate the trial function over a surface.

Consider a local sub-part of the boundary $\partial\Omega$, of a 3-D solid, denoted as $\partial\Omega_x$, the neighborhood of a point $\mathbf{x}$, which is a local region in the global boundary $\partial\Omega$. To approximate the function u in $\partial\Omega_x$, over a number of scattered points $\{\mathbf{x}_I\}$, $(I = 1,2,...,n)$ (where $\mathbf{x}$ is given, in the global Cartesian coordinates by x_1, x_2 andx_3), the moving least squares approximation $u(\mathbf{x})$ of u, $\forall \mathbf{x} \in \partial\Omega_x$, can be defined by

$$u(\mathbf{x}) = \mathbf{p}^T(\mathbf{x})\mathbf{a}(\mathbf{x}) \quad \forall \mathbf{x} \in \partial\Omega_x \tag{9}$$

where $\mathbf{p}^T(\mathbf{x}) = [p_1(\mathbf{x}), p_2(\mathbf{x}), ..., p_m(\mathbf{x})]$ is a monomial basis of order m; and $\mathbf{a}(\mathbf{x})$ is a vector containing coefficients, which are functions of the global Cartesian coordinates $[x_1, x_2, x_3]$, depending on the monomial basis. They are determined by minimizing a weighted discrete L_2 norm, defined, as:

$$\begin{aligned} J(\mathbf{x}) &= \sum_{i=1}^{m} w_i(\mathbf{x})[\mathbf{p}^T(\mathbf{x}_i)\mathbf{a}(\mathbf{x}) - \hat{u}_i]^2 \\ &\equiv [\mathbf{P}\cdot\mathbf{a}(\mathbf{x}) - \hat{\mathbf{u}}]^T\mathbf{W}[\mathbf{P}\cdot\mathbf{a}(\mathbf{x}) - \hat{\mathbf{u}}] \end{aligned} \tag{10}$$

where $w_i(\mathbf{x})$ are the weight functions and $\hat{u}_i$are the fictitious nodal values.

The stationarity of J in Eq. (10), with respect to $\mathbf{a}(\mathbf{x})$ leads to following linear relation between $\mathbf{a}(\mathbf{x})$ and $\hat{\mathbf{u}}$,

$$\mathbf{A}(\mathbf{x})\mathbf{a}(\mathbf{x}) = \mathbf{B}(\mathbf{x})\hat{\mathbf{u}} \tag{11}$$

where matrices $\mathbf{A}(\mathbf{x})$ and $\mathbf{B}(\mathbf{x})$ are defined by

$$\mathbf{A}(\mathbf{x}) = \mathbf{P}^T\mathbf{W}\mathbf{P} \quad \mathbf{B}(\mathbf{x}) = \mathbf{P}^T\mathbf{W} \quad \forall \mathbf{x} \in \partial\Omega_x \tag{12}$$

The MLS approximation is well defined only when the matrix $\mathbf{A}(\mathbf{x})$ in Eq. (11) is non-singular. It needs to be reconditioned, if the monomial basis defined in the global Cartesian coordinate system for an approximation of u as in Eq. (9), becomes nearly linearly dependent on a 3-D surface. One may define a local set of orthogonal coordinates, x'_i as in Figure 1, on $\partial\Omega_x$. One may rewrite Eq. (9) as:

$$\begin{aligned} u = &[1; x_1; x_2; x_3; x_1^2; x_2^2; x_3^2; x_1x_2; x_2x_3; x_3x_1; ...] \\ &[a_1(\mathbf{x}); a_2(\mathbf{x}); a_3(\mathbf{x}); a_4(\mathbf{x}); ...]^T \\ \equiv &[1; x'_1; x'_2; x'_3; x'^2_1; x'^2_2; x'^2_3; x'_1x'_2; x'_2x'_3; x'_3x'_1; ...] \\ &[a'_1(\mathbf{x}); a'_2(\mathbf{x}); a'_3(\mathbf{x}); a'_4(\mathbf{x}); ...]^T \\ &\text{for } \forall \mathbf{x} \in \partial\Omega_x \end{aligned} \tag{13}$$

Suppose $\partial\Omega_x$ becomes nearly planar, which may be defined in the local-set of orthogonal coordinates , for instance, as $x'_3 =$ constant. It is then clear that the monomial basis in Eq. (13), in terms of becomes linearly dependent. In fact, one may make the basis to be *linearly indepent* again in Eq. (13), for instance, for $x'_3 =$ constant, by setting the corresponding coefficients $a'(\mathbf{x})$ to be zero. When this is done, the order of the vector $\mathbf{p}'(\mathbf{x})$ is correspondingly reduced; and thus, correspondingly, the order of $\mathbf{A}(\mathbf{x})$ in Eq. (11) is reduced. Thus, it can be seen that if one proceeds with a full monomial basis, with m basis functions in x_i coordinates in Eq. (9), and if the points on $\partial\Omega_x$ are not all in the same plane, the matrix $\mathbf{A}(\mathbf{x})$ in Eq. (11) will have the full rank of m. One the other hand, if $\partial\Omega_x$ becomes almost planar, say normal to x'_3, then the rank of $\mathbf{A}(\mathbf{x})$ is clearly only $(m-n)$, where n is the reduction in the number of basis due to the fact that $x'_3 =$ constant. Thus, by simply monitoring the eigen-values of $\mathbf{A}(\mathbf{x})$, and if a set of eigen-values becomes nearly or precisely zero, we automatically detect that $\partial\Omega_x$ is becoming nearly planar. In addition, it implies that the normal to the surface can be determined from the lowest eigenvalue of matrix $\mathbf{A}(\mathbf{x})$ when it is singular or nearly-singular, without the local geometry information. It makes the present method to be truly meshless, which does need any background cells to define the geometry as well as the normal direction, if the boundary integrals are handled based on the nodal influence domain [Atluri, Han, and Shen (2003)].

Once coefficients $\mathbf{a}(\mathbf{x})$ in Eq. (11) are determined, one may obtain the approximation from the nodal values at the local scattered points, by substituting them into Eq. (9), as

$$u(\mathbf{x}) = \mathbf{\Phi}^T(\mathbf{x})\hat{\mathbf{u}} \quad \forall \mathbf{x} \in \partial\Omega_x \tag{14}$$

where $\mathbf{\Phi}(\mathbf{x})$ is the so-called shape function of the MLS approximation, defined as,

$$\mathbf{\Phi}(\mathbf{x}) = \mathbf{p}^T(\mathbf{x})\mathbf{A}^{-1}(\mathbf{x})\mathbf{B}(\mathbf{x}) \tag{15}$$

The weight function in Eq. (10) defines the range of influence of node I. Normally it has a compact support. The possible choices are the Gaussian and spline weight functions with compact supports, which have been fully studied in Atluri and Shen (2002a).

It should be pointed out that the shape functions given in Eq. (15) are based on the fictitious nodal values. This

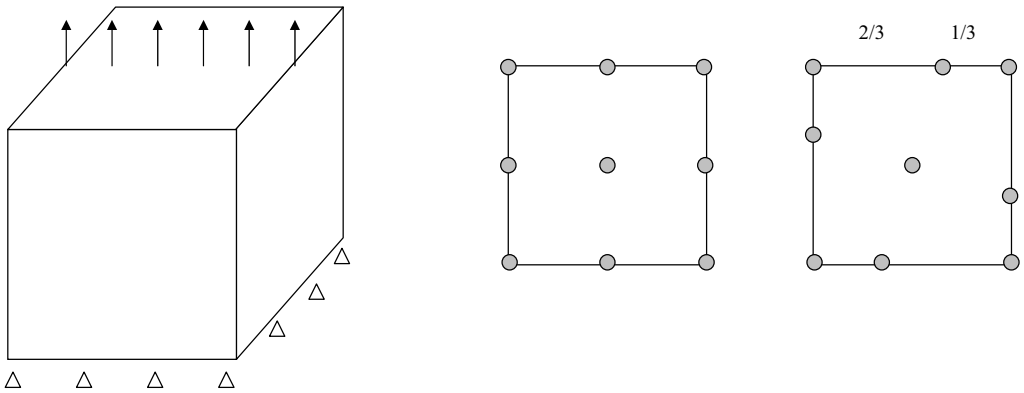

Figure 2 : A cube under uniform tension, and its nodal configurations

introduces an additional complication, since all the nodal values in BIEs are the direct boundary values, a situation which is totally different from the domain meshless methods. As a practical way, a conversion matrix is used to map the fictitious values to true values and applied to the system equations.

4 Numerical Experiments

Several problems in three-dimensional linear elasticity are solved to illustrate the effectiveness of the present method. The numerical results of the MLPG/BIE6 method as applied to problems in 3D elasto-statics, specifically (i) a cube, (ii) a hollow sphere, (iii) a concentrated load on a semi-infinite space, and (iv) non-planar fatigue growth of an elliptical crack, are discussed.

4.1 Cube under uniform tension

The first example is the standard patch test, shown in Figure 2. A cube under the uniform tension is considered. The material parameters are taken as $E = 1.0$, and $\nu = 0.25$. All six faces are modeled with the same configurations with 9 nodes. Two nodal configurations are used for the testing purpose: one is regular and another is irregular, as shown in Figure 2. In the patch tests, the uniform tension stress is applied on the upper face and the proper displacement constraints are applied to the lower face.

The satisfaction of the patch test requires that the displacements are linear on the lateral faces, and are constant on the upper face; and the stresses are constant on all faces. It is found that the present method passes the patch tests. The maximum numerical errors are 1.7×10^{-7} and 3.5×10^{-7} for two nodal configurations, respectively, which may be limited by the computer.

4.2 3D Lamé problem

The 3D Lame problem consists of a hollow sphere under internal pressure, as illustrated in Figure 3. The geometry is defined with the inner and outer radius of 1.0 and 4.0, respectively. The Young's modulus is chosen as and the Poisson ratio . The internal pressure is applied. The inner and outer surfaces are modeled with 772 nodes in the present analysis.

The radial displacement field is given in [Timoshenko &

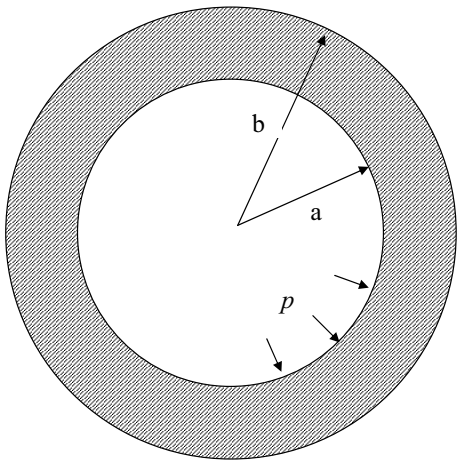

Figure 3 : A hollow sphere under internal pressure (Lame problem)

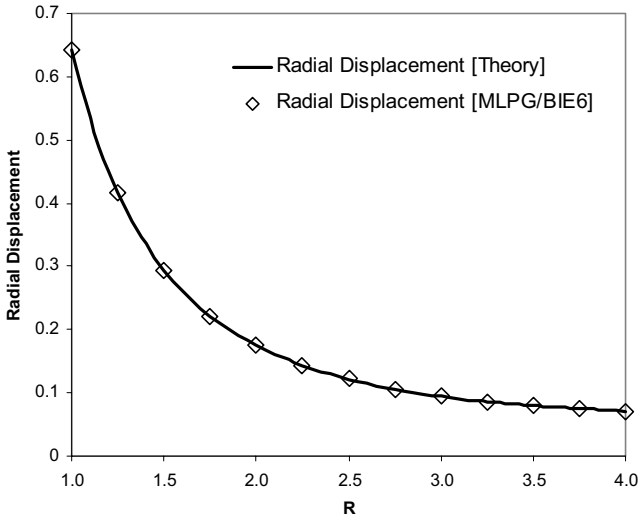

Figure 4 : Internal radial displacement for the Lame problem

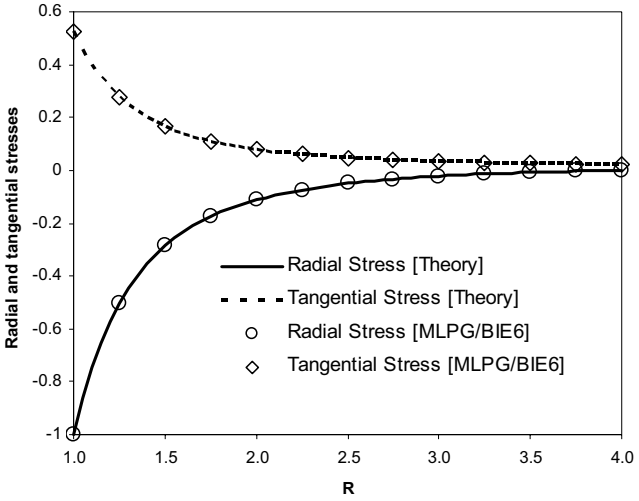

Figure 5 : Internal radial and tangential stresses for the Lame problem

Goodier (1976)],

$$u_r = \frac{pRa^3}{E(b^3-a^3)}\left[(1-2\nu)+(1+\nu)\frac{b^3}{2R^3}\right] \tag{16}$$

The radial and tangential stresses are

$$\sigma_r = \frac{pa^3(b^3-R^3)}{R^3(a^3-b^3)}$$

$$\sigma_\theta = \frac{pa^3(b^3+2R^3)}{2R^3(b^3-a^3)} \tag{17}$$

The displacements are shown in Figure 4, and are compared with the analytical solution. As shown in Figure 5, the radial and tangential stresses are compared with the analytical solution. They agree with each other very well.

4.3 A concentrated load on a semi-infinite space (Boussinesq problem)

The Boussinesq problem can simply be described as a concentrated load acting on a semi-infinite elastic medium with no body force, as shown in Figure 6. Because of its strong singularity, it is difficult for mesh-based domain methods without special treatments. As one of the MLPG domain methods, MLPG5 was applied to this problem in [Li, Shen, Han and Atluri (2003)]. We solve this problem here by using the MLPG/BIE methods to handle the strong singularity. A circular surface with a radius of 20 is used to simulate the semi-infinite space. It is modeled alternatively with two nodal configurations, as shown in Figure 7: one has 649 nodes and another has 1417 nodes. Young's modulus and Poisson's ratio are chosen to be 1.0 and 0.25, respectively.

The exact displacement field within the semi-infinite

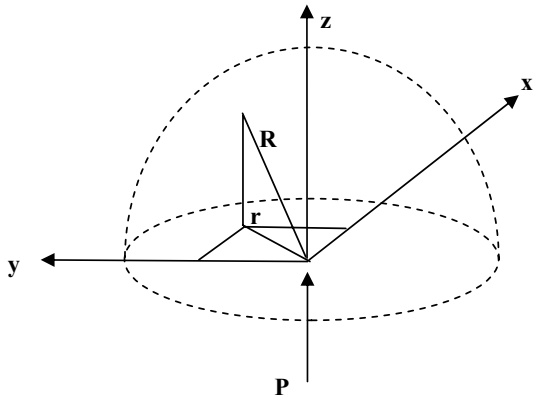

Figure 6 : A concentrated load on a semi-infinite space (Bossinesq Problem)

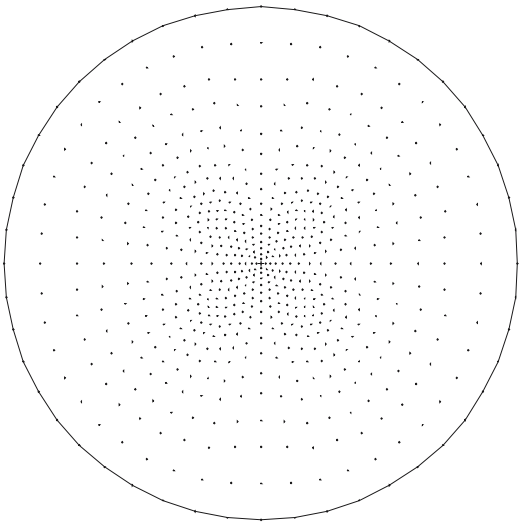

(a)

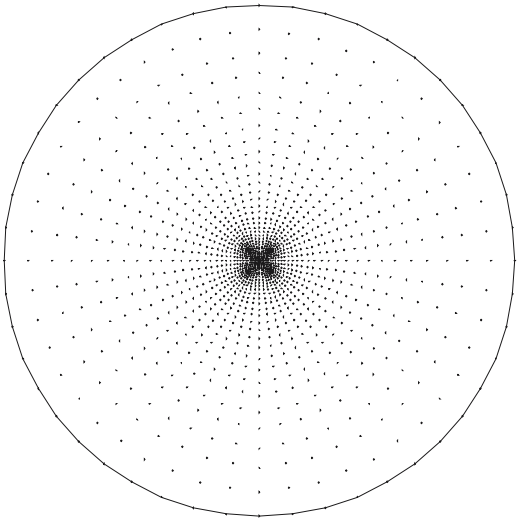

(b)

Figure 7 : two nodal configurations for the Bossinesq Problem: (a) 672 nodes, and (b) 1417 nodes

medium is given in [Timoshenko & Goodier (1976)],

$$u_r = \frac{(1+\nu)P}{2E\pi R}\left[\frac{zr}{R^2} - \frac{(1-2\nu)r}{R+z}\right]$$

$$u_w = \frac{(1+\nu)P}{2E\pi R}\left[\frac{z^2}{R^2} + 2(1-\nu)\right] \tag{18}$$

where u_r is the radial displacement, and u_w is the vertical one, R is the distance to the loading point, r is the projection of R on the loading surface.

The theoretical stresses field is:

$$\sigma_r = \frac{P}{2\pi R^2}\left[-\frac{3r^2 z}{R^3} + \frac{(1-2\nu)R}{R+z}\right]$$

$$\sigma_\theta = \frac{(1-2\nu)P}{2\pi R^2}\left[\frac{z}{R} - \frac{R}{R+z}\right]$$

$$\sigma_z = -\frac{3Pz^3}{2\pi R^5}$$

$$\tau_{zr} = \tau_{rz} = -\frac{3\,\mathrm{Pr}\,z^2}{2\pi R^5} \tag{19}$$

It is clear that the displacements and stresses are strongly singular and approach to infinity; with the displacement being $O(1/R)$ and the stresses being $O(1/R^2)$.

The vertical displacement u_w alone the z-axis is shown in Figure 8, and the radial and tangential stresses are shown in Figure 9 and Figure 10. The analytical solution for the displacement and stress are plotted on the same figures for comparison purpose. The zoom-in views within the shorter distance from the loading point are also shown in each figure. The shortest distance is 0.0025, where is very close the loading point and displacement and stresses increase rapidly. It can be clearly seen that both the MLPG/BIE displacement and stress results match the analytical solution very well, even within the very short distance, from the point of load application.

4.4 Non-planar Crack Growth

An inclined elliptical crack with semi-axes c and a, subjected to fatigue loading, is shown in Figure 11. Its orientation is characterized by an angle, α. This problem has been solved by using the boundary element method in [Nikishkov, Park, J.H., Atluri, S. N. (2001)] but it was reported that only K_I was obtained with the satisfactory agreement with the theoretical solution while failing in K_{II} and K_{III}. The present meshless method is applied to solve this problem, again. The nodal configuration is used to model the crack inclined at 45 degrees with 249 nodes, as shown in Figure 12. The exact solution for a tensile loading σ is given in [Tada, Paris and Irwin

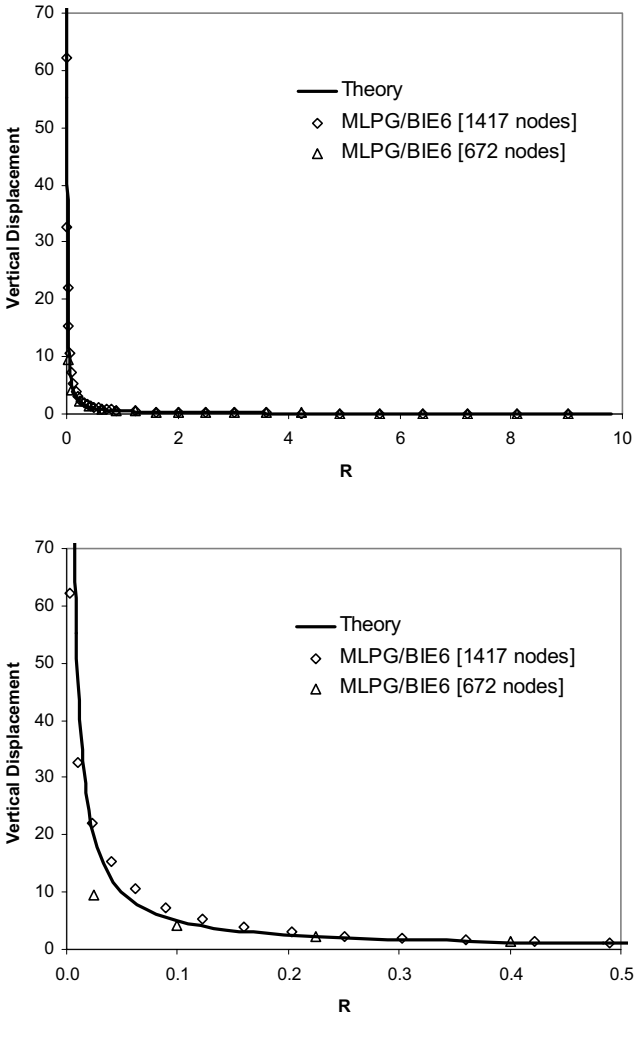

Figure 8 : Vertical displacement alone z-axis for the Bossinesq problem

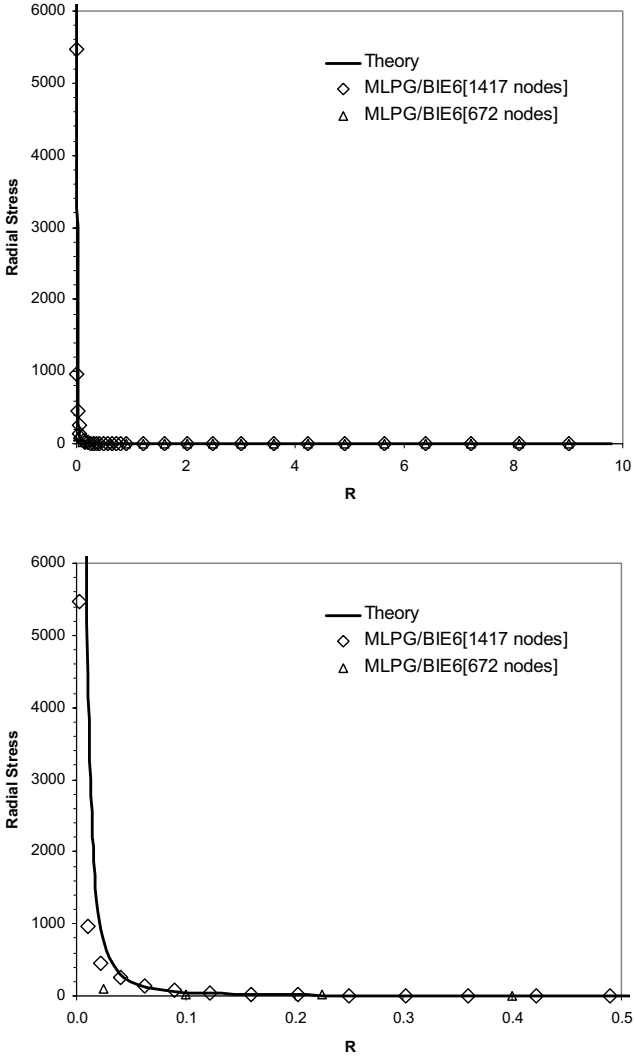

Figure 9 : Radial stress alone z-axis for the Bossinesq problem

(2000)]:

$$K_I = K_0(1+\cos 2\alpha)\frac{1}{E(k)}f(\varphi)$$

$$K_{II} = K_0 \sin 2\alpha \frac{k^2(a/c)}{B}\frac{\cos\varphi}{f(\varphi)}$$

$$K_{III} = K_0 \sin 2\alpha \frac{k^2(1-\nu)}{B}\frac{\sin\varphi}{f(\varphi)} \qquad (20)$$

where φ is the elliptical angle and

$$K_0 = \frac{\sigma\sqrt{\pi a}}{2}$$

$$f(\varphi) = (\sin^2\varphi + (a/c)^2\cos^2\varphi)^{1/4}$$

$$k^2 = 1-(a/c)^2$$

$$B = (k^2-\nu)E(k) + \nu(a/c)^2 K(k) \qquad (21)$$

The elliptical integrals of the first and second kind, $E(k)$

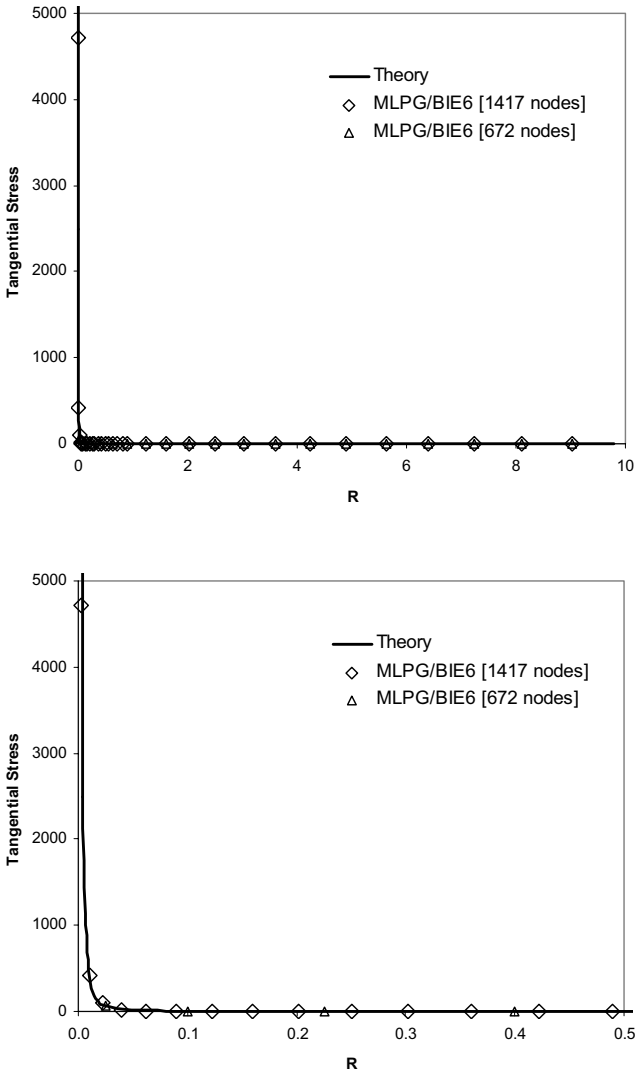

Figure 10 : Tangential stress alone z-axis for the Bossinesq problem

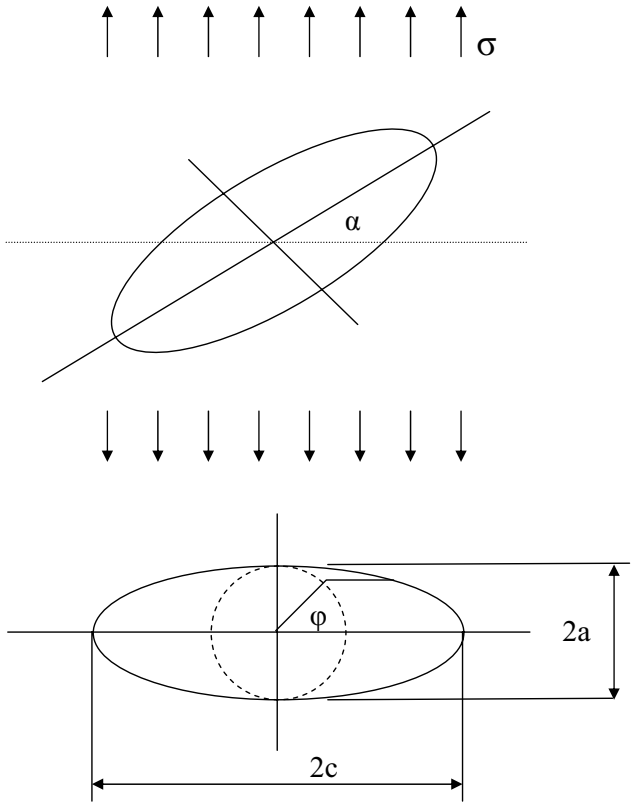

Figure 11 : Inclined elliptical crack under tension

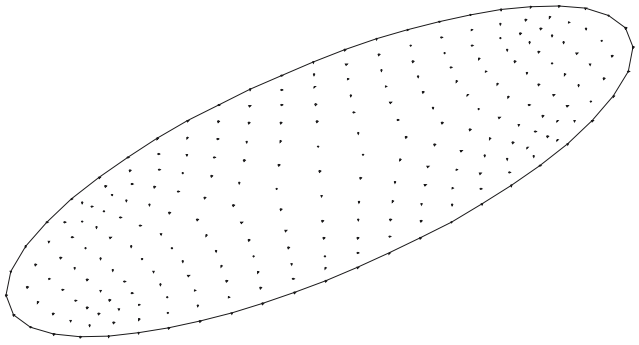

Figure 12 : Nodal configuration for an inclined elliptical crack

and $K(k)$, are defined as

$$K(k) = \int_0^{\pi/2} \frac{d\theta}{\sqrt{1-k^2\sin^2\theta}}$$

$$E(k) = \int_0^{\pi/2} \sqrt{1-k^2\sin^2\theta}\, d\theta \qquad (22)$$

As a mixed-mode crack, the distribution of all three stress intensity factors, K_I, K_{II} and K_{III}, along the crack front are shown in Figure 13, after being normalized by K_0 as defined in Eq. (21). It can be seen that a good agreement of the present numerical results with the theoretical solution is obtained.

The fatigue growth is also performed for this inclined crack. The Paris model is used to simulate fatigue crack growth. The crack growth rate with respect to the loading

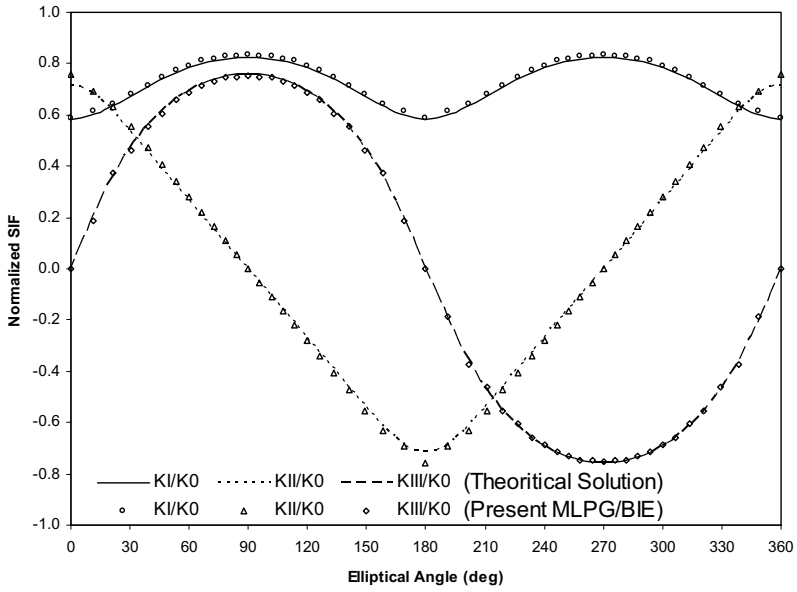

Figure 13 : Normalized stress intensity factors along the crack front of an inclined elliptical crack under tensile load

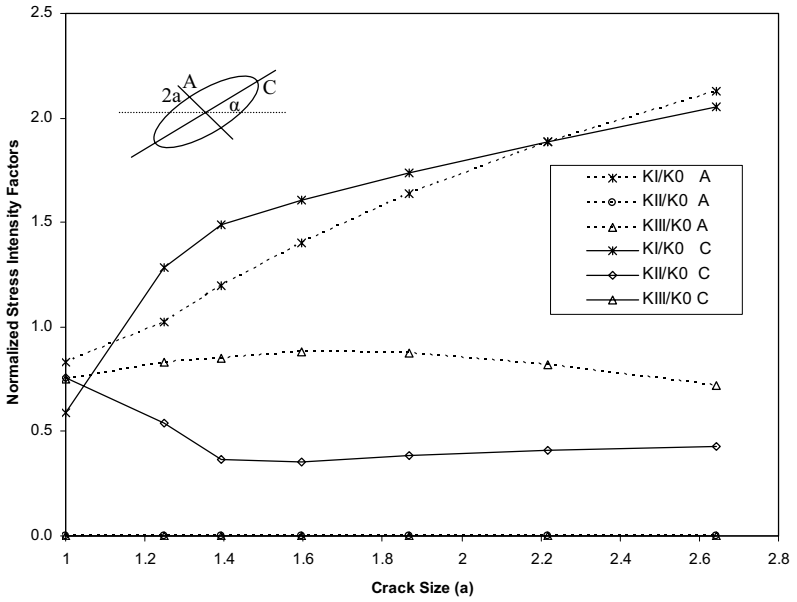

Figure 14 : Normalized stress intensity factors for the mixed-mode fatigue growth of an inclined elliptical crack

cycles, da/dN, is defined as:

$$\frac{da}{dN} = C(\Delta K_{eff})^n \tag{23}$$

in which the material parameters C and n are taken for 7075 Aluminum as $C = 1.49 \times 10^{-8}$ and $n = 3.21$ [Nikishkov, Park and Atluri(2001)]. The crack growth is simulated by adding nodes along the crack front. The newly added points are determined through the K solutions. Seven increments are performed to grow the crack from the initial size $a = 1$ to the final size $a = 2.65$. The normalized stress intensity factors during the crack growing are given in Figure 14, which are also normalized by K_0 in Eq. (21). The results show that K_I keeps increasing while K_{II} and K_{III} are decreasing during the crack growth. It confirms that this mixed-mode crack

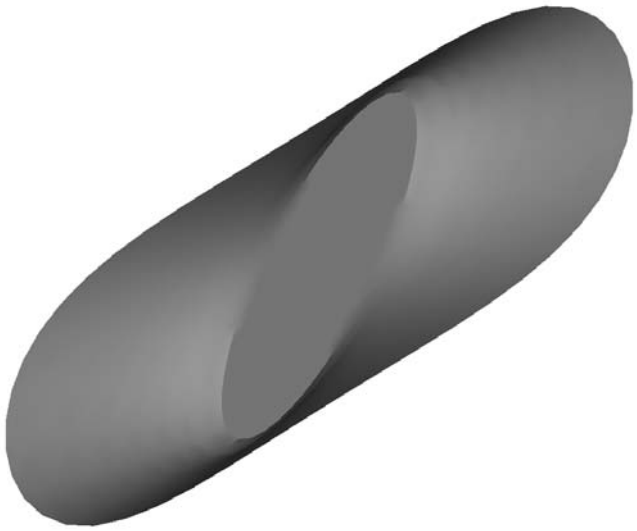

Figure 15 : Final shape of an inclined elliptical crack after mixed-model growth

becomes a mode-I dominated one, while growing. The shape of the final crack is shown in Figure 15. It is clear that while the crack, in its initial configuration, starts out as a mixed-mode crack; and after a substantial growth, the crack configuration is such that it is in a pure mode-I state.

5 Closure

In this paper, we numerically implemented the specific symmetric form of "Meshless Local Petrov-Galerkin BIE Method" (MLPG/BIE6). It is one of the general MLPG/BIE methods, which are derived for displacement and traction BIEs, by using the concept of the general meshless local Petrov-Galerkin (MLPG) approach developed in Atluri et al [1998, 2002a,b, 2003]. The MLS surface-interpolation, with the use of Cartesian coordinates, is enhanced for the three dimensional surface without the requirement of a mesh or cells, to define the local geometry. It leads to the truly meshless BIE methods with the use of the nodal influence domain for the boundary integrations. The accuracy and efficiency of the present MLPG approach are demonstrated with numerical results.

Acknowledgement: This work was supported through a cooperative research agreement between the US Army Research Labs, and the University of California, Irvine, through the US Army Research Office. Dr. R. Namburu is the cognizant program official. The many helpful discussions with Drs. R. Namburu, and A. M. Rajendran, are thankfully acknowledged.

References

Atluri, S. N. (1985): Computational solid mechanics (finite elements and boundary elements) present status and future directions, *The Chinese Journal of Mechanics*.

Atluri, S. N.; Han, Z. D.; Shen, S. (2003): Meshless Local Patrov-Galerkin (MLPG) approaches for weakly-singular traction & displacement boundary integral equations, *CMES: Computer Modeling in Engineering & Sciences*, vol. 4, no. 5, pp. 507-517.

Atluri, S. N.; Shen, S. (2002a): The meshless local Petrov-Galerkin (MLPG) method. Tech. Science Press, 440 pages.

Atluri, S. N.; Shen, S. (2002b): The meshless local Petrov-Galerkin (MLPG) method: A simple & less-costly alternative to the finite element and boundary element methods. *CMES: Computer Modeling in Engineering & Sciences*, vol. 3, no. 1, pp. 11-52

Atluri, S. N.; Zhu, T. (1998): A new meshless local Petrov-Galerkin (MLPG) approach in computational mechanics. *Computational Mechanics.*, Vol. 22, pp. 117-127.

Cruse, T. A.; Richardson, J. D. (1996): Non-singular Somigliana stress identities in elasticity, *Int. J. Numer. Meth. Engng.*, vol. 39, pp. 3273-3304.

Fung, Y. C; Tong, P. (2001): Classical and Computational Solid Mechanics, World Scientific, 930 pages.

Gaul, L.; Fischer, M.; Nackenhorst, U. (2003): FE/BE Analysis of Structural Dynamics and Sound Radiation from Rolling Wheels, *CMES: Computer Modeling in Engineering & Sciences*, vol. 3, no. 6, pp. 815-824.

Gowrishankar, R.; Mukherjee S. (2002): A 'pure' boundary node method for potential theory, *Comminucations in Numerical Methods*, vol. 18, pp. 411-427.

Han. Z. D.; Atluri, S. N. (2002): SGBEM (for Cracked Local Subdomain) – FEM (for uncracked global Structure) Alternating Method for Analyzing 3D Surface Cracks and Their Fatigue-Growth, *CMES: Computer Modeling in Engineering & Sciences*, vol. 3, no. 6, pp. 699-716.

Han. Z. D.; Atluri, S. N. (2003): On Simple For-

mulations of Weakly-Singular Traction & Displacement BIE, and Their Solutions through Petrov-Galerkin Approaches, *CMES: Computer Modeling in Engineering & Sciences*, vol. 4 no. 1, pp. 5-20.

Hatzigeorgiou, G. D.; Beskos, D. E. (2002): Dynamic Response of 3-D Damaged Solids and Structures by BEM, *CMES: Computer Modeling in Engineering & Sciences*, vol. 3, no. 6, pp. 791-802.

Li, G.; Aluru, N. R. (2003): A boundary cloud method with a cloud-by-cloud polynomial basis, *Engineering Analysis with Boundary Elements*, vol. 27, pp. 57-71.

Muller-Karger, C. M.; Gonzalez, C.; Aliabadi, M. H.; Cerrolaza, M. (2001): Three dimensional BEM and FEM stress analysis of the human tibia under pathological conditions, *CMES: Computer Modeling in Engineering & Sciences*, vol.2, no.1, pp.1-14.

Nikishkov, G. P.; Park, J. H.; Atluri, S. N. (2001): SGBEM-FEM alternating method for analyzing 3D non-planar cracks and their growth in structural components, *CMES: Computer Modeling in Engineering & Sciences*, vol.2, no.3, pp.401-422.

Okada, H.; Atluri, S. N. (1994): Recent developments in the field-boundary element method for finite/small strain elastoplasticity, *Int. J. Solids Struct.* vol. 31 n. 12-13, pp. 1737-1775.

Okada, H.; Rajiyah, H.; Atluri, S. N. (1989)a: A Novel Displacement Gradient Boundary Element Method for Elastic Stress Analysis with High Accuracy, *J. Applied Mech.*, April 1989, pp. 1-9.

Okada, H.; Rajiyah, H.; Atluri, S. N. (1989)b: Non-hyper-singular integral representations for velocity (displacement) gradients in elastic/plastic solids (small or finite deformations), *Computational. Mechanics.*, vol. 4, pp. 165-175.

Okada, H.; Rajiyah, H.; Atluri, S. N. (1990): A full tangent stiffness field-boundary-element formulation for geometric and material non-linear problems of solid mechanics, *Int. J. Numer. Meth. Eng.*, vol. 29, no. 1, pp. 15-35.

Tada, H.; Paris, P. C.; Irwin, G. R. (2000): *The Stress Analysis of Cracks Handbook*, ASME Press.

Timoshenko, S. P.; Goodier, J. N. (1976): Theory of Elasticity, 3^{rd} edition, McGraw Hill.

Tsai, C. C.; Young, D. L.; Cheng, A. H.-D. (2002): Meshless BEM for Three-dimensional Stokes Flows, *CMES: Computer Modeling in Engineering & Sciences*, vol.3, no.1, pp. 117-128.

Wen, P. H.; Aliabadi, M. H.; Young, A. (2003): Boundary Element Analysis of Curved Cracked Panels with Mechanically Fastened Repair Patches, *CMES: Computer Modeling in Engineering & Sciences*, vol. 3, no. 1, pp. 1-10.

Zhang, J. M.; Yao, Z. H. (2001): Meshless regular hybrid boundary node method. *CMES: Computer Modeling in Engineering & Sciences*, vol.2, no.3, pp.307-318.

Appendix

The displacement solution corresponding to this unit point load is given by the Galerkin-vector-displacement-potential:

$$\boldsymbol{\varphi}^{*p} = (1-\upsilon)F^{*}\mathbf{e}^{p} \tag{24}$$

The corresponding displacements are derived from the Galerkin-vector-displacement- potential as:

$$u_i^{*p}(\mathbf{x},\xi) = (1-\upsilon)\delta_{pi}F^{*}_{,kk} - \frac{1}{2}F^{*}_{,pi} \tag{25}$$

The gradients of the displacements are:

$$u^{*p}_{i,j}(\mathbf{x},\xi) = (1-\upsilon)\delta_{pi}F^{*}_{,kkj} - \frac{1}{2}F^{*}_{,pij} \tag{26}$$

The corresponding stresses are given by:

$$\begin{aligned}\sigma^{*p}_{ij}(\mathbf{x},\xi) &\equiv E_{ijkl}u^{*p}_{k,l} \\ &= \mu[(1-\upsilon)\delta_{pi}F^{*}_{,kkj} + \upsilon\delta_{ij}F^{*}_{,pkk} - F^{*}_{,pij}] \\ &+ \mu(1-\upsilon)\delta_{pj}F^{*}_{,kki}\end{aligned} \tag{27}$$

Three functions ϕ^{*p}_{ij}, G^{*p}_{ij}, Σ^{*}_{ijpq} and H^{*}_{ijpq} are defined as [Han and Atluri (2003)]

$$\phi^{*p}_{ij}(\mathbf{x},\xi) \equiv -\mu(1-\upsilon)\delta_{pj}F^{*}_{,kki} \tag{28}$$

$$G^{*p}_{ij}(\mathbf{x},\xi) = \mu[(1-\upsilon)e_{ipj}F^{*}_{,kk} - e_{ikj}F^{*}_{,pk}] \tag{29}$$

$$\Sigma^{*}_{ijpq}(\mathbf{x},\xi) = E_{ijkl}e_{nlp}\sigma^{*k}_{nq}(\mathbf{x},\xi) \tag{30}$$

$$\begin{aligned}&H^{*}_{ijpq}(\mathbf{x},\xi) \\ &= \mu^2[-\delta_{ij}F_{,pq} + 2\delta_{ip}F_{,jq} + 2\delta_{jq}F_{,ip} - \delta_{pq}F_{,ij} \\ &- 2\delta_{ip}\delta_{jq}F_{,bb} + 2\upsilon\delta_{iq}\delta_{jp}F_{,bb} + (1-\upsilon)\delta_{ij}\delta_{pq}F_{,bb})]\end{aligned} \tag{31}$$

For 3D problems,

$$F^* = \frac{r}{8\pi\mu(1-\upsilon)} \tag{32}$$

where $r = \|\xi - \mathbf{x}\|$

$$u_i^{*p}(\mathbf{x},\xi) = \frac{1}{16\pi\mu(1-\upsilon)r}[(3-4\upsilon)\delta_{ip} + r_{,i}r_{,p}] \tag{33}$$

$$G_{ij}^{*p}(\mathbf{x},\xi) = \frac{1}{8\pi(1-\upsilon)r}[(1-2\upsilon)e_{ipj} + e_{ikj}r_{,k}r_{,p}] \tag{34}$$

$$\sigma_{ij}^{*p}(\mathbf{x},\xi) = \frac{1}{8\pi(1-\upsilon)r^2} [(1-2\upsilon)(\delta_{ij}r_{,p} - \delta_{ip}r_{,j} - \delta_{jp}r_{,i}) - 3r_{,i}r_{,j}r_{,p}] \tag{35}$$

$$H_{ijpq}^*(\mathbf{x},\xi) = \frac{\mu}{8\pi(1-\upsilon)r}[4\upsilon\delta_{iq}\delta_{jp} - \delta_{ip}\delta_{jq} - 2\upsilon\delta_{ij}\delta_{pq} + \delta_{ij}r_{,p}r_{,q} + \delta_{pq}r_{,i}r_{,j} - 2\delta_{ip}r_{,j}r_{,q} - \delta_{jq}r_{,i}r_{,p}] \tag{36}$$

For 2D problems,

$$F^* = \frac{-r^2\ln r}{8\pi\mu(1-\upsilon)} \tag{37}$$

$$u_i^{*p}(\mathbf{x},\xi) = \frac{1}{8\pi\mu(1-\upsilon)}[-(3-4\upsilon)\ln r\delta_{ip} + r_{,i}r_{,p}] \tag{38}$$

$$G_{ij}^{*p}(\mathbf{x},\xi) = \frac{1}{4\pi(1-\upsilon)} [-(1-2\upsilon)\ln r\, e_{ipj} + e_{ikj}r_{,k}r_{,p}] \tag{39}$$

$$\sigma_{ij}^{*p}(\mathbf{x},\xi) = \frac{1}{4\pi(1-\upsilon)r} [(1-2\upsilon)(\delta_{ij}r_{,p} - \delta_{ip}r_{,j} - \delta_{jp}r_{,i}) - 2r_{,i}r_{,j}r_{,p}] \tag{40}$$

$$H_{ijpq}^*(\mathbf{x},\xi) = \frac{\mu}{4\pi(1-\upsilon)}[-4\upsilon\ln r\delta_{iq}\delta_{jp} + \ln r\delta_{ip}\delta_{jq} + 2\upsilon\ln r\delta_{ij}\delta_{pq} \quad + \delta_{ij}r_{,p}r_{,q} + \delta_{pq}r_{,i}r_{,j} - 2\delta_{ip}r_{,j}r_{,q} - \delta_{jq}r_{,i}r_{,p}] \tag{41}$$